View Article Online
View Journal

Green Chemistry

Cutting-edge research for a greener sustainable future

Accepted Manuscript

This article can be cited before page numbers have been issued, to do this please use: L. Gräber, V. MARANGON, M. Kumar, M. Weil and D. Bresser, *Green Chem.*, 2025, DOI: 10.1039/D5GC00252D.

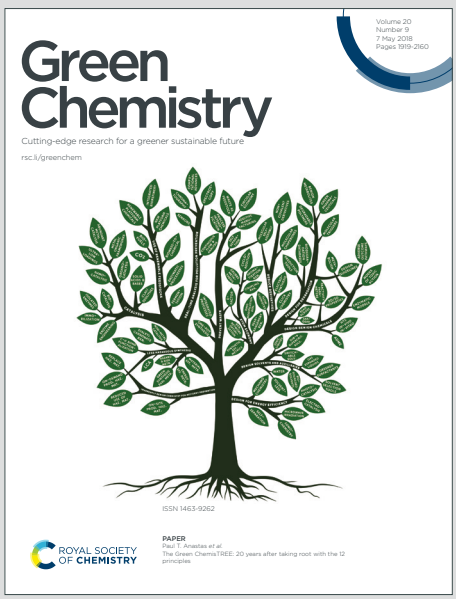

ROYAL SOCIETY OF CHEMISTRY

rsc.li/greenchem

Green Foundation

View Article Online
DOI: 10.1039/D5GC00252D

1. This work proposes a new single-ion conducting polymer electrolyte relying on a sustainable, completely fluorine-free composition to achieve safer high-performance lithium batteries.
2. The polymer electrolyte is prepared via a simple synthesis route with yield values of well above 75%. The inclusion of non-toxic polyacrylonitrile allows for the preparation of self-standing electrolyte membranes. Li‖$LiFePO_4$ cells exploiting this new electrolyte and fluorine-free cathodes provide stable cycling for more than 500 cycles and good performance even when increasing the active material loading to almost 10 mg cm^{-2}.
3. Future research will focus on further increasing the active material mass loading and the substitution of lithium metal with alternative anode materials to obtain intrinsically safe, truly sustainable, low-cost, high-performance lithium-ion polymer batteries.

Fluorine-free Polysiloxane-based Single-Ion Conducting Polymer Electrolyte for Lithium-Metal Batteries

View Article Online
DOI: 10.1039/D5GC00252D

Leo Gräber[†,‡], Vittorio Marangon[†,‡,*], Manish Kumar[†,‡] , Marcel Weil[†,‡], and Dominic Bresser[†,‡,§,*]

[†]*Helmholtz Institute Ulm (HIU), Helmholtzstrasse 11, 89081 Ulm, Germany*

[‡]*Karlsruhe Institute of Technology (KIT), P.O. Box 3640, 76021 Karlsruhe, Germany*

[§] *Ulm University (UUlm), 89069 Ulm, Germany*

Keywords: fluorine-free; polysiloxane; single-ion conductor; polymer electrolyte; lithium battery

***Corresponding authors:** vittorio.marangon@kit.edu ; dominic.bresser@kit.edu

View Article Online
DOI: 10.1039/D5GC00252D

Abstract

Herein, the synthesis and comprehensive characterization of a new, completely fluorine-free single-ion conducting polymer electrolyte (SIPE) for lithium-metal batteries is reported. For this new SIPE, lithium(4-styrenesulfonyl)(dicyanomethide) has been grafted onto a polysiloxane backbone. Self-standing membranes containing additionally non-toxic polyacrylonitrile and propylene carbonate reveal suitable mechanical properties, high ionic conductivity of more than 10^{-4} S cm^{-1}, and a good anodic stability exceeding 4.1 V vs. Li^+/Li at 40 °C. Symmetric Li‖Li cells show an excellent cycle life with more than 1,000 h of lithium stripping and plating, thanks to the formation of a stable and low resistive interphase. As a result, also completely fluorine-free Li‖$LiFePO_4$ cells provide stable cycling for more than 500 cycles, rendering this new electrolyte system very promising for the realization of more sustainable and safer lithium batteries.

View Article Online
DOI: 10.1039/D5GC00252D

Introduction

Lithium-ion batteries (LIBs) are often acknowledged as key-technology to drive a successful clean-energy transition due to their highly versatile applications, especially in portable electronic devices, electric vehicles and grid-storage plants.[1–3] However, after extensive research, the specific capacity of LIBs relying on graphite- or silicon-based anodes is about to reach the theoretical limits.[4,5] The replacement of the anode with metallic lithium is expected to significantly increase the energy density due to its superior capacity and negative potential (3861 mAh g^{-1}, -3.040 V vs. SHE).[6–8] However, lithium-metal batteries (LMBs) face serious challenges, particularly in regard to the formation of a stable solid electrolyte interphase (SEI) on the lithium surface and safety.[8–10] The latter is undermined by the risk of dendrite formation, which can lead to short circuits and thermal runaway of the cell.[11,12] Thus, the stabilization of the Li│electrolyte interface is mandatory for a widespread commercialization of LMBs.[13,14] Several strategies were implemented to address this issue, including host structures for the Li metal electrode,[15,16] the design of artificial SEIs,[17,18] and the utilization of solid electrolytes, e.g. sulfides,[19–21] ceramics[22,23] or polymers.[7,24–28] The latter represents a promising approach as polymers provide concomitantly high safety, the potential low-cost synthesis from abundant starting materials, good processability, and favorable mechanical properties.[29,30] Nevertheless, a key issue is represented by the ionic conductivity, which usually ranges between 10^{-5} and 10^{-7} S cm^{-1}, i.e., well below the conductivity of liquid electrolytes (□10^{-3} S cm^{-1}).[24–26] Additionally, conventional salt-in-polymer electrolytes suffer from a significantly higher mobility of the anions compared to the lithium cations, resulting in a very low lithium transference number (t_{Li^+} < 0.5).[31] This limits the cell performance owing to the potential buildup of reversed polarization gradients, which may cause uneven deposition of lithium, promoting dendrite formation.[32–34] A possible solution resides in the utilization of single-ion conducting polymer electrolytes (SIPEs), in which the negative charge carrier is a weakly coordinating anion, covalently bonded to or incorporated in the polymer chain.[24,35] In particular, highly fluorinated sulfonates and sulfonylimides deriving from the widely used lithium bis(trifluoromethanesulfonyl)imide (as conducting salt) are

View Article Online
DOI: 10.1039/D5GC00252D

usually preferred due to the relevant charge delocalization triggered by the strongly electron-withdrawing sulfonyl- and trifluoromethane-units,[35–38] while fluorine allows for the formation of a LiF-rich SEI which reportedly improves the cell performance.[39–41] Moreover, fluorinated compounds usually offer improved thermal and electrochemical stability with respect to the F-free homologous.[40,41] However, the toxicity and persistency of fluorinated materials pose serious concerns about their production costs and recycling, leading to major obstacles to the sustainability of the related devices.[42,43] Thus, many efforts have been recently focused on the development of novel F-free anions designed to retain the desirable properties of traditional fluorinated conducting salts for LIBs and LMBs, relying for examples on borates,[43,44] phosphates,[45] or cyanides.[46,47] Despite the remarkable progresses achieved in this field, to the best of our knowledge, only a handful of reports proposed the development of fluorine-free SIPEs,[47–49] where the new electrolytes are usually applied in batteries relying on modest active material loadings at the cathode or on the use of harmful solvents for the electrode processing.

Following this objective, we report herein the development of a novel fluorine-free SIPE exploiting the weakly coordinating lithium (4-styrenesulfonyl)(dicyanomethide) (LiSDM),[47] which is grafted via a thiol-ene click reaction to a thiol-functionalized polysiloxane backbone poly[(mercaptopropyl)methylsiloxane] (PMMS) following a previous work, in which we used lithium (3-methacryloyloxypropylsulfonyl)(trifluoromethylsulfonyl)imide as ionic side chain.[50] To yield self-standing, flexible, but still fluorine-free polymer electrolyte membranes, the resulting ionomer is blended with polyacrylonitrile (PAN) instead of the commonly used polyvinylidene fluoride (PVdF).[51] Swollen with 50 wt.% of propylene carbonate (PC), these SIPE membranes provide high ionic conductivity, long-term stable lithium stripping and plating for more than 1,000 h, and good performance in Li‖$LiFePO_4$ (LFP) cells, which are realized with a completely F-free configuration by substituting the commonly employed PVdF binder in the cathode by sodium carboxymethyl cellulose (CMC), allowing for the aqueous processing of the electrode. In addition, the possible scale-up of this novel configuration is explored by realizing LFP mass loadings of up to

View Article Online
DOI: 10.1039/D5GC00252D

9 mg cm^{-2}, benefitting from the incorporation of the F-free SIPE into the electrode to enhance the electrode | electrolyte interfacial contact and ionic conductivity within the electrode. Finally, a toxicity assessment of the F-free SIPE membrane is provided, comparing the herein developed F-free SIPE with an earlier reported F-containing SIPE. This comparison highlights the great progresses towards the realization of less toxic electrolytes and provides a benchmark for future developments. Moreover, the work presented herein highlights the need to carefully evaluate any potential improvement concerning sustainability, going well beyond a "simple" judgement based on the absence of certain elements – even if highly desirable.

Results and Discussion

The synthesis of LiSDM and SIPE is schematically depicted in **Figure 1**a. The LiSDM ionic side-chain is synthesized by nucleophilic substitution of malononitrile on freshly prepared (4-styrene)sulfonylchloride in the presence of a base. The acidic proton of the methide side reacts further with aqueous LiOH as a strong base to form the lithiated LiSDM. Both the ^{1}H and ^{13}C NMR spectra (**Figure 1**b and **Figure S1**, respectively) confirm the successful synthesis of LiSDM in agreement with previous literature.[47] Additionally, the FTIR spectrum in **Figure 1**c displays the characteristic bands for C=C at 920 cm^{-1},[52] the symmetric and anti-symmetric O=S=O stretching at 1140 and 1300 cm^{-1}, respectively,[50,53] and the C≡N stretching at 2190 cm^{-1}, while the band at 2225 cm^{-1} is induced by the interaction of Li^{+} with the cyano group, leading to the favorized formation of the C=C=N^{-}iminium-type mesomeric structure.[54,55] The successful synthesis of the final SIPE, prepared by a thiol-ene click reaction between LiSDM and PMMS using azobisisobutyronitrile (AiBN) as a radical starter (**Figure 1**a), is revealed by ^{1}H NMR and FTIR spectroscopy (**Figure 1**b and **Figure 1**c, respectively). In particular, the FTIR data show the preservation of the aforementioned bands for O=S=O and C≡N, while two additional peaks arise at 779 and 1073 cm^{-1}, ascribed to Si-O-Si bonds.[50,52] The successful transition from LiSDM to the eventual SIPE is further corroborated by the aliphatic C-H bonds identified at 2920 cm^{-1}.[50,52] The molecular weight of the final SIPE is

View Article Online
DOI: 10.1039/D5GC00252D

determined via gel permeation chromatography (GPC) revealing a molecular mass of about 10-14 kg mol^{-1} (M_n and M_w are provided in **Table S1**).

Polymer electrolyte membranes were obtained by blending the SIPE with various contents of PAN (15, 25, 35, 45 and 55 wt.%) to ensure proper mechanical stability. The final membranes were indicated as B15, B25, B35, B45, and B55 (see the corresponding composition and a photograph in **Table S2** and **Figure S2**, respectively). The decomposition temperature of the B15-B55 membranes is determined via TGA (**Figure S3**a) and compared with that of the neat SIPE and bare PAN in **Figure 2**a, where the decomposition temperature is defined as the value at which a mass loss of 3 wt.% was detected. The comparison reveals a relevant dependance between the decomposition temperature and the PAN content, as expected by the wide difference between the values recorded for SIPE and bare PAN, i.e., 120 and 285 °C, respectively. In particular, the decomposition temperatures display a quasi-logarithmic increase from B15 to B55 with respective values of 127, 167, 193, 216, and 223 °C. This trend may be associated with modifications in microstructure and morphology of the polymer blends linked to the increase of PAN content, which gradually drives the thermal behavior from a response similar to SIPE (B15) to an intermediate one between SIPE and PAN (B55).[56,57] Prior to the electrochemical measurements, the membranes were swollen with PC (50 wt.% with respect to the membrane as determined via Equation S1 and TGA in **Figure S3**b), serving as "molecular transporter" owing to its high dielectric constant to improve the ionic conductivity. **Figure 2**b evaluates the anodic stability of the membranes determined via linear sweep voltammetry (LSV) showing values between 4.1 and 4.3 V vs. Li^+/Li (the limiting potential values are determined in correspondence to an evolving current of 2.5 μA cm^{-2}), with no apparent influence of the PAN content, though a higher PAN content appears generally favorable. In fact, the anodic stability is expected to be determined by the oxidizable thioether function in SIPE,[50,58] while the minor signal observed for all the membranes slightly above 4.0 V vs. Li^+/Li may be ascribed to the presence of PC.[50] Although the addition of fluorinated species such as PVdF may relevantly increase the anodic stability,[25,59,60] the F-free configuration proposed herein represents a more sustainable solution and

View Article Online
DOI: 10.1039/D5GC00252D

still allows for the application in LMBs exploiting cathodes operating at moderate voltage like LFP.40

The ionic conductivity (σ) is presented in the form of an Arrhenius plot in **Figure 2**c (see the corresponding Nyquist plots in **Figure S4**). The comparison reveals the lowest σ for B15 between 5.4×10^{-6} and 3.8×10^{-4} S cm^{-1} in the 10 – 90 °C range, followed by B55 and B45, while B25 exhibits values slightly lower than those associated to B35, which delivers the best σ between 1.0×10^{-4} and 9.2×10^{-4} S cm^{-1}. This behavior may be due to an optimal microstructure of the B35 blend, while maintaining a suitable concentration of Li^+ cations. At 40 °C B35 exhibits an ionic conductivity of 2.9×10^{-4} S cm^{-1}, which appears suitable for a potential commercial application of such SIPE-based electrolytes.[32] The compatibility of the membranes with metallic lithium was evaluated through Li stripping/plating tests in symmetric Li‖Li cells by galvanostatic cycling at increasing current densities (see **Figure S5**). The overall trend is displayed in **Figure 2**d, revealing the expected increase in overpotential for all the electrolytes for an increasing current density, with the lowest overpotential values for B35, i.e., from □4.3 to ~208 mV in the 2.5 – 100 μA cm^{-2} current density range. Considering the above results, especially in terms of σ and overpotential, B35 has been selected as the most promising candidate for the forthcoming experiments.

The structure and morphology of the dry B35 membrane were investigated via X-ray diffraction (XRD) and scanning electron microscopy (SEM) coupled with energy dispersive X-ray spectroscopy (EDX). The XRD patterns recorded for bare PAN, the SIPE powder, and the B35 membrane, as presented in **Figure S6**, reveal for the latter the combination of the amorphous SIPE, as indicated by the broad reflection centered around 19°,[61] and the partially crystalline nature of PAN, as indicated by the retention of the prominent reflection at 17°, which has been attributed to the planar spacing of the polymer chains,[62,63] while its intensity is substantially reduced. The homogeneous blending of the SIPE and PAN is evidenced by the SEM-EDX analyses presented in **Figure 3**a-f. The SEM micrographs (**Figure 3**a,b) display a homogeneous and smooth surface of the B35 membrane, without any indication of agglomerates, along with the presence of sub-micrometric pores that may favor the uptake of the PC molecules. The EDX mapping of silicon, nitrogen, sulfur, and carbon confirms a

View Article Online
DOI: 10.1039/D5GC00252D

uniform distribution of these elements, thus, corroborating a successful and homogeneous blending of the two polymers (**Figure 3**c-f).

The Li^+ transference number (t^+) of the B35 membrane is determined using the Bruce-Vincent-Evans method (**Figure S7**).[64,65] The data collected from the chronoamperometric curves and from the fitting of the Nyquist plots recorded before and after polarization (insets in **Figure S7**) are reported in **Table S3**, revealing a t^+ approaching unity for cells with varying thicknesses of the B35 membranes, as expected for SIPEs. The stability of B35 towards the aging in contact with lithium metal is evaluated by electrochemical impedance spectroscopy (EIS) measurements performed on symmetric Li‖Li cells, as displayed in **Figure 3**g (Nyquist plots) and **Figure 3**h (evolution of the electrode│electrolyte interphase resistance, i.e., R_i, see **Table S4** for the actual values). The data reveal a rather stable R_i between 210 and 230 Ω during the first 12 h after cell assembly, while a gradual growth up to 300 Ω is observed after 7 days, indicating the consolidation of a low resistive SEI. The stability of the interphase is further proven by EIS analyses performed on the same cells after galvanostatic Li stripping/plating tests at 10 and 50 μA cm^{-2}, revealing a R_i of about 300 Ω (**Figure S8** and **Table S5**). A magnification of the corresponding voltage profiles (**Figure S8**a) shows a very stable and flat voltage response, further corroborating the single-ion conducting behavior in agreement with the Li^+ transference number of essentially unity. In addition, the long-term galvanostatic Li stripping/plating test depicted in **Figure 3**i demonstrates the ability of B35 to withstand an extensive cycling in symmetric Li‖Li cells over 1,000 h at 50 μA cm^{-2}, maintaining a rather stable overpotential of less than 130 mV during the whole experiment. A magnification of the Li stripping/plating voltage profiles is reported in **Figure S9**, showing a very minor slope of the generally square-shaped profiles, which likely originates from a somewhat slower Li^+ transport across the SEI layer on the lithium-metal electrodes.[66]

The B35 membrane is subsequently evaluated in completely fluorine-free Li‖LFP cells. **Figure 4** displays the rate capability tests. The rate capability tests are performed with LFP electrodes having two different active material mass loadings of either 2.8 ± 0.2 mg cm^{-2} or 8.2 ± 0.2 mg cm^{-2}, with the

View Article Online
DOI: 10.1039/D5GC00252D

latter incorporating 7 wt.% of dry SIPE. The cells are galvanostatically cycled at increasing C-rates from 0.05C to 2C (1C = 170 mA g^{-1}). The cycling trend in **Figure 4**a displays for both the LFP cathodes a remarkable discharge capacity in the 145-155 mAh g^{-1} range at 0.05C (i.e., 85 – 91 % of the theoretical capacity), with subsequent minor decay as demonstrated by the capacity of 134 mAh g^{-1} delivered at 0.2C. In addition, the low-loading LFP cathode still displays a capacity of 111 mAh g^{-1} and 74 mAh g^{-1} at 0.5C and 1C, respectively, and both the electrodes retrieve a capacity around 130 mAh g^{-1} when the current is lowered back to 0.2C after 30 cycles. The dis-/charge profiles related to the low-loading LFP cathode (**Figure 4**b) display the first charge at 0.05C centered at ~3.46 V (de-lithiation of LFP) followed by a sloping discharge curve at ~3.39 V (lithiation of LFP),[67] while an increase of polarization can be observed in concomitance with the rising of the current as expected by the ohmic resistance increment, despite the cell still presents electrochemical activity at the relatively high current of 2C. Notably, the voltage profiles related to the high-loading LFP cathode (**Figure 4**c) show only slightly higher polarization at 0.05C for charge/discharge processes, occurring at ~3.46 and ~3.36 V, respectively, while reveal almost total deactivation of the electrochemical process already at 0.5C indicating a rate capability extended up to 0.2C.

Long-term galvanostatic cycling tests of Li │ B35 │ LFP cells are depicted in **Figure 5**. The low mass loading LFP cathodes (around 2.8 mg cm^{-2}) were subjected to measurements either at 0.2C or 0.5C, while the LFP cathodes with a mass loading of about 9.2 mg cm^{-2} were cycled at 0.2C. The cycling trends reveal a maximum capacity of 137 mAh g^{-1} retained at the 93% after 150 cycles for the low-loading electrode cycled at 0.2C (**Figure 5**a), while the one cycled at 0.5C displays a cycle life up to 500 cycles with maximum capacity of 133 mAh g^{-1} retained at the 73% at the end of the test (**Figure 5**b). The high-loading LFP cathode exhibits instead a delivered capacity around 120 mAh g^{-1} retained at the 75% after 70 cycles. In addition, all the cells demonstrate a CE exceeding 99% after the first cycle, subsequently maintained for the entire measurement. The lower initial CE observed for all the tests can be ascribed to the consolidation of the passivation layers, which would also explain the gradual increase of capacity during the first cycles. The corresponding voltage profiles (**Figure 5**d-f)

View Article Online
DOI: 10.1039/D5GC00252D

show for all the tests the development of the single-plateau charge/discharge processes, including the expected increase in polarization when a higher C rate (i.e., 0.5C in **Figure 5**e) or a high mass loading cathode (**Figure 5**f) are used. To investigate the capacity decay upon long-term cycling in more detail, EIS was performed. **Figure 5**g shows the Nyquist plots recorded for Li │ B35 │ LFP cells upon cycling at 0.5C with LFP electrodes having an active material loading of 2.8 mg cm^{-2}. The corresponding trend for R_i as function of the cycle number, obtained by NLLS fitting (see **Table S6** for the actual data), is reported in **Figure 5**h. The analysis reveals an increase of the interphase resistance during the three activation cycles from 317 to 327 Ω and a subsequent drop to 257 Ω for the 5th cycle and to 217 Ω for the 25th cycle, which is in line with the initial growth of a resistive passivation layer, which then stabilizes and becomes less resistive upon cycling. Subsequently, R_i shows a steady, though minor increase up to 300 Ω after 200 cycles. This behavior matches with the trend of the delivered capacity exhibited by these cells, as displayed in **Figure 5**b, which shows a slight decrease after the first cycle, a gradual growth and stabilization during the following ~75 cycles, and a steady decrease until the end of the test. These reactions are apparently more pronounced when cycling the cells at elevated temperatures and in the absence of F, which commonly results in the formation of very well passivating LiF,[10] while operating the cells at lower temperatures of, e.g., 20 °C results in a significantly lower specific capacity owing to a substantially higher polarization and interfacial resistance (**Figure S10**). Nonetheless, a comparison with other, comparable studies reported earlier[25,48,68–72] (**Table S7**) reveals that the results achieved in this work are well comparable with the state of the art, especially when taking into account the considerably higher active material mass loading of the LFP electrodes studied herein, the absence of F,[25,68–72] and the lower cycling temperature with respect to other F-free configurations.[48]

To underline the great impact of transitioning to F-free SIPEs with regard to an enhanced sustainability, we conducted a hazard and toxicity assessment (**Appendix 1**) and compared this with an earlier reported F-containing SIPE using the same polysiloxane backbone (PSiOM; **Appendix 2**).[50] For this purpose, we used the hazard traffic light (HTL) method to identify potential

View Article Online
DOI: 10.1039/D5GC00252D

hotspots in the synthesis process. The SIPE membrane synthesis process shows multiple potential health hazards, including acute toxicity impacts (H300, H311, H331), skin corrosion/irritation (H314), serious eye damage/irritation (H318)), carcinogenicity (H350), and reproductive toxicity (H360), in particular associated with the precursors *N,N*-dimethylformamid, thionylchloride, tert-butylcatechol, acetonitrile, triethylamine, and lithiumhydroxid monohydrate for the synthesis of the (4-styrene)sulfonylchloride and the synthesis of the LiSDM ionic side-chain. Physical hazards (flammable liquid, (H225)) are also associated with a few solvents (acetonitrile, triethylamine, and tetrahydrofurane) used for the synthesis of the LiSDM ionic side-chain and the synthesis of the SIPE as such. However, the synthesis of the F-containing analogous PSiOM[50] provides similar potential health and physical hazards deriving from the use of flammable liquids (H225), acute toxicity (H301, H311, H331), skin corrosion (H314), serious eye damage/irritation (H318), carcinogenicity (H350), reproductive toxicity (H360), including in addition aspiration hazard (H304), and specific organ toxicity due to repetitive exposure (H372). Thus, critical hotspots in the synthesis of the F-free SIPE still remain, in particular for the synthesis of the LiSDM ionic side-chain. Nevertheless, the F-containing PSiOM counterpart exhibits additional HTL impacts, a higher number of hazardous chemicals involved in the synthesis sub-processes (about 30% more), and the concerns linked to the environmental challenges deriving from the F-containing species such as trifluoromethanesulfonamide, PVdF-co-hexafluoropropylene (PVdF-HFP), and fluoroethylene carbonate; the latter two being used for the preparation of the polymer electrolyte membranes.[50] In this context, **Figure 6** summarises the number of hazards based on the HTL results (see **Appendix 1** and **Appendix 2** for the details) linked to the synthesis of both polymer electrolytes in terms of physical (**Figure 6**a), health (**Figure 6**b), and total overall hazards (**Figure 6**c), showing the general lower number of hazards for the F-free SIPE compared to the F-containing PSiOM. It is worth noting that data gaps in this case include the absence of hazard statements for poly(mercaptopropyl) methylsiloxane, PAN, and PVdF-HFP, which were not included in the HTL assessment. These gaps prevent a proper comparison between the electrolytes in terms of environmental hazards, which were

View Article Online
DOI: 10.1039/D5GC00252D

thereby excluded from **Figure 6**, and make the calculation of quantitative total hazard points (THP) presently not meaningful. Nevertheless, the given toxicity assessment highlights the remaining challenges for the synthesis of truly sustainable SIPEs and sets a benchmark for future studies, while also evidencing the progresses achieved compared to the F-containing counterpart.

Conclusions

Herein, a novel fluorine-free SIPE is synthetized and characterized. The electrolyte membrane benefited of a content of PAN of 35 wt.% and incorporated 50 wt.% of PC solvent as molecular transporter. The self-standing membrane presented at 40 °C a transference number around 1, ionic conductivity over 10^{-4} S cm^{-1} and stability up to 4.2 V vs. Li^+/Li. EIS performed upon aging on Li‖Li cell revealed the growth of an electrode|electrolyte interphase with low resistance, while Li stripping/plating tests showed remarkable cyclability over 1,000 h with corresponding overvoltage as low as 130 mV. Galvanostatic cycling tests on Li‖LFP cells revealed a rate capability up to 1C and a cycle life of 500 cycles for electrodes with active material loading of 2.8 mg cm^{-2}, and capacities approaching 120 mAh g^{-1} when a loading as high as 9.2 mg cm^{-2} was used. The performances achieved herein are comparable to previously reported fluorinated SIPEs, and may thus pave the way towards the development of well-performing, safe and environmentally friendly polymer electrolytes for LMBs.

Supporting Information

Photographic image and additional experimental data including ^{13}C NMR spectra, TGA profiles, Nyquist plots recorded by EIS, voltage profiles related to Li stripping/plating tests and chronoamperometric curves (DOC).

View Article Online
DOI: 10.1039/D5GC00252D

Acknowledgement

The authors would like to acknowledge financial support by the Federal Ministry of Education and Research (BMBF) within the FB2-Poly project (03XP0429B), as well as the financial support by the Helmholtz Association.

References

1 A. Z. Al Shaqsi, K. Sopian and A. Al-Hinai, *Energy Rep.*, 2020, **6**, 288–306.

2 D. Larcher and J.-M. Tarascon, *Nat. Chem.*, 2015, **7**, 19–29.

3 J. B. Goodenough and Y. Kim, *Chem. Mater.*, 2010, **22**, 587–603.

4 T. Kim, W. Song, D.-Y. Son, L. K. Ono and Y. Qi, *J. Mater. Chem. A*, 2019, **7**, 2942–2964.

5 J. Xu, X. Cai, S. Cai, Y. Shao, C. Hu, S. Lu and S. Ding, *ENERGY Environ. Mater.*, 2023, **6**, e12450.

6 S. Xia, X. Wu, Z. Zhang, Y. Cui and W. Liu, *Chem*, 2019, **5**, 753–785.

7 H. Wang, L. Sheng, G. Yasin, L. Wang, H. Xu and X. He, *Energy Storage Mater.*, 2020, **33**, 188–215.

8 A. Varzi, K. Thanner, R. Scipioni, D. Di Lecce, J. Hassoun, S. Dörfler, H. Altheus, S. Kaskel, C. Prehal and S. A. Freunberger, *J. Power Sources*, 2020, **480**, 228803.

9 H. Wu, H. Jia, C. Wang, J. Zhang and W. Xu, *Adv. Energy Mater.*, 2021, **11**, 2003092.

10 X. He, D. Bresser, S. Passerini, F. Baakes, U. Krewer, J. Lopez, C. T. Mallia, Y. Shao-Horn, I. Cekic-Laskovic, S. Wiemers-Meyer, F. A. Soto, V. Ponce, J. M. Seminario, P. B. Balbuena, H. Jia, W. Xu, Y. Xu, C. Wang, B. Horstmann, R. Amine, C.-C. Su, J. Shi, K. Amine, M. Winter, A. Latz and R. Kostecki, *Nat. Rev. Mater.*, 2021, **6**, 1036–1052.

11 L. He, Q. Sun, L. Lu and S. Adams, *ACS Appl. Mater. Interfaces*, 2021, **13**, 34320–34331.

12 X. Zhang, A. Wang, X. Liu and J. Luo, *Acc. Chem. Res.*, 2019, **52**, 3223–3232.

View Article Online
DOI: 10.1039/D5GC00252D

13 M. K. Aslam, Y. Niu, T. Hussain, H. Tabassum, W. Tang, M. Xu and R. Ahuja, *Nano Energy*, 2021, **86**, 106142.

14 D. Wang, W. Zhang, W. Zheng, X. Cui, T. Rojo and Q. Zhang, *Adv. Sci.*, 2017, **4**, 1600168.

15 Y. Cheng, J. Chen, Y. Chen, X. Ke, J. Li, Y. Yang and Z. Shi, *Energy Storage Mater.*, 2021, **38**, 276–298.

16 H. Liu, J. Di, P. Wang, R. Gao, H. Tian, P. Ren, Q. Yuan, W. Huang, R. Liu, Q. Liu and M. Feng, *Carbon Energy*, 2022, **4**, 654–664.

17 H. Zhang, G. G. Eshetu, X. Judez, C. Li, L. M. Rodriguez-Martínez and M. Armand, *Angew. Chem. Int. Ed.*, 2018, **57**, 15002–15027.

18 R. S. Thompson, D. J. Schroeder, C. M. López, S. Neuhold and J. T. Vaughey, *Electrochem. Commun.*, 2011, **13**, 1369–1372.

19 Z. Ge, N. Chen, R. Wang, R. Ma, B. Fan, D. Le Coq, X. Zhang, H. Ma and B. Xue, *Chem. Eng. J.*, 2023, **467**, 143409.

20 N. T. Temesgen, H. K. Bezabh, M. A. Weret, K. N. Shitaw, Y. Nikodimos, B. W. Taklu, K. Lakshmanan, S.-C. Yang, S.-K. Jiang, C.-J. Huang, S.-H. Wu, W.-N. Su and B. J. Hwang, *J. Power Sources*, 2023, **556**, 232462.

21 Y. Wu, J. Xu, P. Lu, J. Lu, L. Gan, S. Wang, R. Xiao, H. Li, L. Chen and F. Wu, *Adv. Energy Mater.*, 2023, **13**, 2301336.

22 X. Zhang, J. Wang, D. Hu, W. Du, C. Hou, H. Jiang, Y. Wei, X. Liu, F. Jiang, J. Sun, H. Yuan and X. Huang, *Energy Storage Mater.*, 2024, **65**, 103089.

23 Mauger, Julien, Paolella, Armand, and Zaghib, *Materials*, 2019, **12**, 3892.

24 A. Mayer, D. Steinle, S. Passerini and D. Bresser, *Nanotechnology*, 2022, **33**, 062002.

25 X. Dong, Z. Chen, X. Gao, A. Mayer, H.-P. Liang, S. Passerini and D. Bresser, *J. Energy Chem.*, 2023, **80**, 174–181.

26 Z. Song, F. Chen, M. Martinez-Ibañez, W. Feng, M. Forsyth, Z. Zhou, M. Armand and H. Zhang, *Nat. Commun.*, 2023, **14**, 4884.

View Article Online
DOI: 10.1039/D5GC00252D

27 J. Chattopadhyay, T. S. Pathak and D. M. F. Santos, *Polymers*, 2023, **15**, 3907.

28 X. Zhao, C. Wang, H. Liu, Y. Liang and L. Fan, *Batter. Supercaps*, 2023, **6**, e202200502.

29 P. Lennartz, B. A. Paren, A. Herzog-Arbeitman, X. C. Chen, J. A. Johnson, M. Winter, Y. Shao-Horn and G. Brunklaus, *Joule*, 2023, **7**, 1471–1495.

30 V. Marangon, L. Minnetti, E. Barcaro and J. Hassoun, *Chem. – Eur. J.*, 2023, **29**, e202301345.

31 K. Timachova, H. Watanabe and N. P. Balsara, *Macromolecules*, 2015, **48**, 7882–7888.

32 M. Doyle, T. F. Fuller and J. Newman, *Electrochimica Acta*, 1994, **39**, 2073–2081.

33 X.-G. Sun and J. B. Kerr, *Macromolecules*, 2006, **39**, 362–372.

34 K. M. Diederichsen, E. J. McShane and B. D. McCloskey, *ACS Energy Lett.*, 2017, **2**, 2563–2575.

35 C. Shan, Y. Wang, M. Liang, K. Lu, C. Xiong, W. Hu and B. Liu, *Energy Storage Mater.*, 2023, **63**, 102955.

36 H. Yuan, J. Luan, Z. Yang, J. Zhang, Y. Wu, Z. Lu and H. Liu, *ACS Appl. Mater. Interfaces*, 2020, **12**, 7249–7256.

37 S. Kondou, M. Abdullah, I. Popov, M. L. Martins, L. A. O'Dell, H. Ueda, F. Makhlooghiazad, A. Nakanishi, T. Sudoh, K. Ueno, M. Watanabe, P. Howlett, H. Zhang, M. Armand, A. P. Sokolov, M. Forsyth and F. Chen, *J. Am. Chem. Soc.*, 2024, **146**, 33169–33178.

38 D. Fraile-Insagurbe, N. Boaretto, I. Aldalur, I. Raposo, F. J. Bonilla, M. Armand and M. Martínez-Ibañez, *Nano Res.*, 2023, **16**, 8457–8468.

39 Z. Chen, D. Steinle, H.-D. Nguyen, J.-K. Kim, A. Mayer, J. Shi, E. Paillard, C. Iojoiu, S. Passerini and D. Bresser, *Nano Energy*, 2020, **77**, 105129.

40 G. Hernández, R. Mogensen, R. Younesi and J. Mindemark, *Batter. Supercaps*, 2022, **5**, e202100373.

41 A. Mayer, H.-D. Nguyen, A. Mariani, T. Diemant, S. Lyonnard, C. Iojoiu, S. Passerini and D. Bresser, *ACS Macro Lett.*, 2022, **11**, 982–990.

42 J. Glüge, M. Scheringer, I. T. Cousins, J. C. DeWitt, G. Goldenman, D. Herzke, R. Lohmann, C. A. Ng, X. Trier and Z. Wang, *Environ. Sci. Process. Impacts*, 2020, **22**, 2345–2373.

View Article Online
DOI: 10.1039/D5GC00252D

43 G. Hernández, A. J. Naylor, Y.-C. Chien, D. Brandell, J. Mindemark and K. Edström, *ACS Sustain. Chem. Eng.*, 2020, **8**, 10041–10052.

44 Z. Jiang, C. Li, T. Yang, Y. Deng, J. Zou, Q. Zhang and Y. Li, *ACS Energy Lett.*, 2024, **9**, 1389–1396.

45 H. Markusson, P. Johansson and P. Jacobsson, *Electrochem. Solid-State Lett.*, 2005, **8**, A215.

46 A. Fu, J. Lin, Z. Zhang, C. Xu, Y. Zou, C. Liu, P. Yan, D.-Y. Wu, Y. Yang and J. Zheng, *ACS Energy Lett.*, 2022, **7**, 1364–1373.

47 M. Martinez-Ibañez, E. Sanchez-Diez, L. Qiao, L. Meabe, A. Santiago, H. Zhu, L. A. O'Dell, J. Carrasco, M. Forsyth, M. Armand and H. Zhang, *Batter. Supercaps*, 2020, **3**, 738–746.

48 C. Han, L. Qiao, G. Xu, G. Chen, K. Chen, S. Zhang, J. Ma, S. Dong, X. Zhou, Y. Han, Z. Cui and G. Cui, *ACS Appl. Mater. Interfaces*, 2024, **16**, 48792–48802.

49 B. R. Johnson, A. Sankara Raman, A. Narla, S. Jhulki, L. Chen, S. R. Marder, R. Ramprasad, K. Turcheniuk and G. Yushin, *ACS Omega*, 2024, **9**, 15410–15420.

50 H. Liang, M. Zarrabeitia, Z. Chen, S. Jovanovic, S. Merz, J. Granwehr, S. Passerini and D. Bresser, *Adv. Energy Mater.*, 2022, **12**, 2200013.

51 X. Zhong, J. Han, L. Chen, W. Liu, F. Jiao, H. Zhu and W. Qin, *Appl. Surf. Sci.*, 2021, **553**, 149564.

52 X. Huang, J.-Y. Guo, J. Yang, Y. Xia, Y.-F. Zhang, P. Fu and F.-P. Du, *Polymer*, 2022, **254**, 125066.

53 S. Zhao, Y. Zhang, H. Pham, J.-M. Y. Carrillo, B. G. Sumpter, J. Nanda, N. J. Dudney, T. Saito, A. P. Sokolov and P.-F. Cao, *ACS Appl. Energy Mater.*, 2020, **3**, 12540–12548.

54 S. Xie, A. Nikolaev, O. A. Nordness, L. C. Llanes, S. D. Jones, P. M. Richardson, H. Wang, R. J. Clément, J. Read De Alaniz and R. A. Segalman, *Macromolecules*, 2022, **55**, 5723–5732.

55 Y. A. Min'ko, N. V. Belina, V. V. Sushev, G. K. Fukin, M. P. Bubnov and A. N. Kornev, *J. Organomet. Chem.*, 2007, **692**, 4157–4160.

56 S. Ramesh, C.-W. Liew, E. Morris and R. Durairaj, *Thermochim. Acta*, 2010, **511**, 140–146.

57 A. C.-Y. Wong and F. Lam, *Polym. Test.*, 2002, **21**, 691–696.

58 A. Mayer, T. Ates, A. Varzi, S. Passerini and D. Bresser, *Front. Chem.*, 2022, **10**, 974202

59 H.-D. Nguyen, G.-T. Kim, J. Shi, E. Paillard, P. Judeinstein, S. Lyonnard, D. Bresser and C. Iojoiu, *Energy Environ. Sci.*, 2018, **11**, 3298–3309.

60 A. Mayer, A. Mariani, X. Dong, G. Vansse, P. Theato, C. Iojoiu, S. Passerini and D. Bresser, *Macromolecules*, 2023, **56**, 2505–2514.

61 M. A. Schiavon, N. A. Armelin and I. V. P. Yoshida, *Mater. Chem. Phys.*, 2008, **112**, 1047–1054.

62 H. Zhang, L. Quan, A. Gao, Y. Tong, F. Shi and L. Xu, *Polymers*, 2020, **12**, 221.

63 M.-J. Yu, Y.-J. Bai, C.-G. Wang, Y. Xu and P.-Z. Guo, *Mater. Lett.*, 2007, **61**, 2292–2294.

64 S. Zugmann, M. Fleischmann, M. Amereller, R. M. Gschwind, H. D. Wiemhöfer and H. J. Gores, *Electrochimica Acta*, 2011, **56**, 3926–3933.

65 J. Evans, C. A. Vincent and P. G. Bruce, *Polymer*, 1987, **28**, 2324–2328.

66 K. Borzutzki, J. R. Nair, M. Winter and G. Brunklaus, *ACS Appl. Mater. Interfaces*, 2022, **14**, 5211–5222.

67 V. Marangon, L. Minnetti, M. Adami, A. Barlini and J. Hassoun, *Energy Fuels*, 2021, **35**, 10284–10292.

68 Q. Pan, S. Jiang, Z. Li, Y. Liu, Y. Du, N. Zhao, Y. Zhang and J.-M. Liu, *J. Membr. Sci.*, 2021, **636**, 119601.

69 Y. Chen, H. Ke, D. Zeng, Y. Zhang, Y. Sun and H. Cheng, *J. Membr. Sci.*, 2017, **525**, 349–358.

70 Y. Chen, C. Li, D. Ye, Y. Zhang, H. Bao and H. Cheng, *J. Membr. Sci.*, 2021, **620**, 118926.

71 K. Deng, S. Wang, S. Ren, D. Han, M. Xiao and Y. Meng, *J. Power Sources*, 2017, **360**, 98–105.

72 C. Li, B. Qin, Y. Zhang, A. Varzi, S. Passerini, J. Wang, J. Dong, D. Zeng, Z. Liu and H. Cheng, *Adv. Energy Mater.*, 2019, **9**, 1803422.

View Article Online
DOI: 10.1039/D5GC00252D

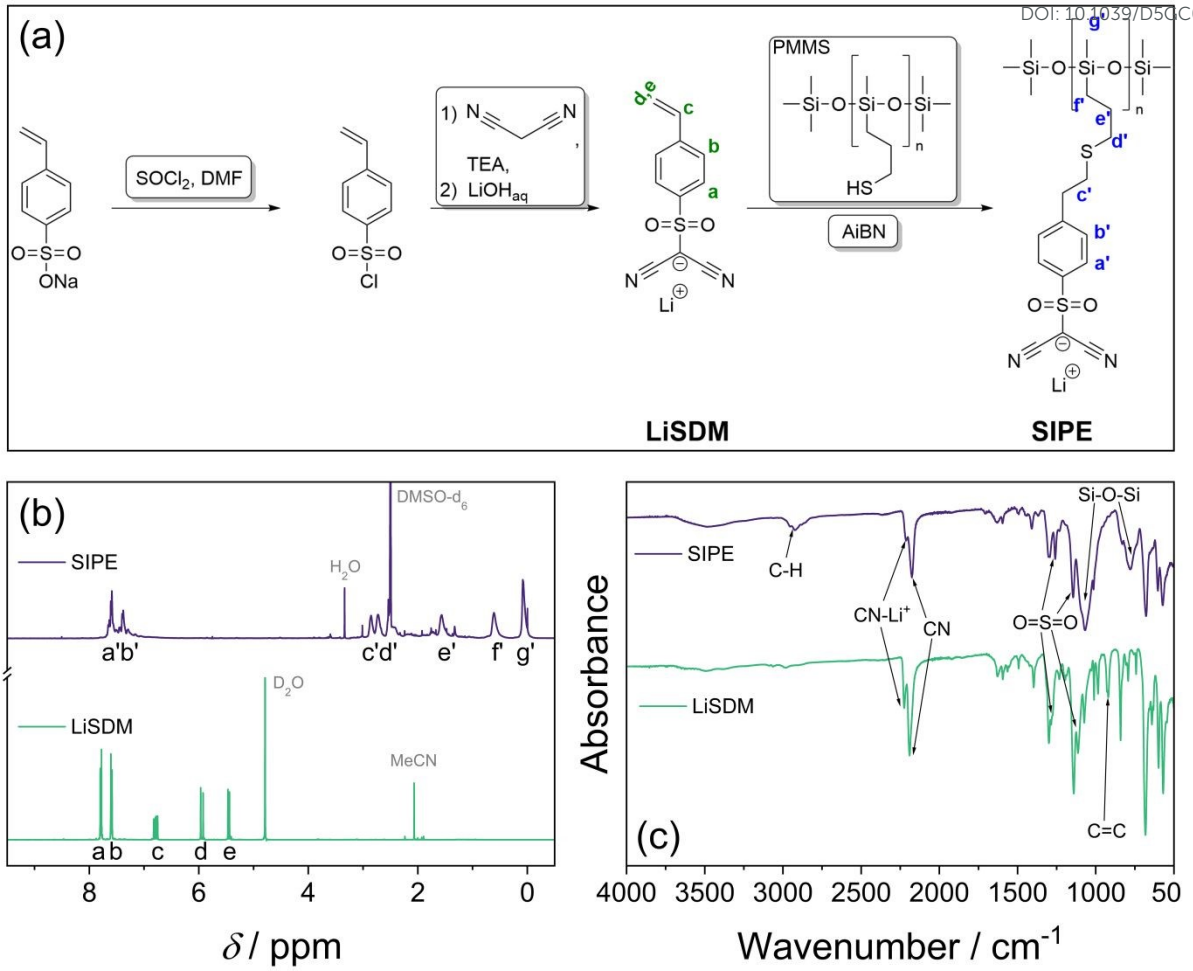

Figure 1. (a) Schematic representation of the synthesis pathway for the fluorine-free SIPE via LiSDM; **(b)** ^{1}H NMR and **(c)** FTIR spectra of LiSDM (green) and SIPE (violet).

View Article Online
DOI: 10.1039/D5GC00252D

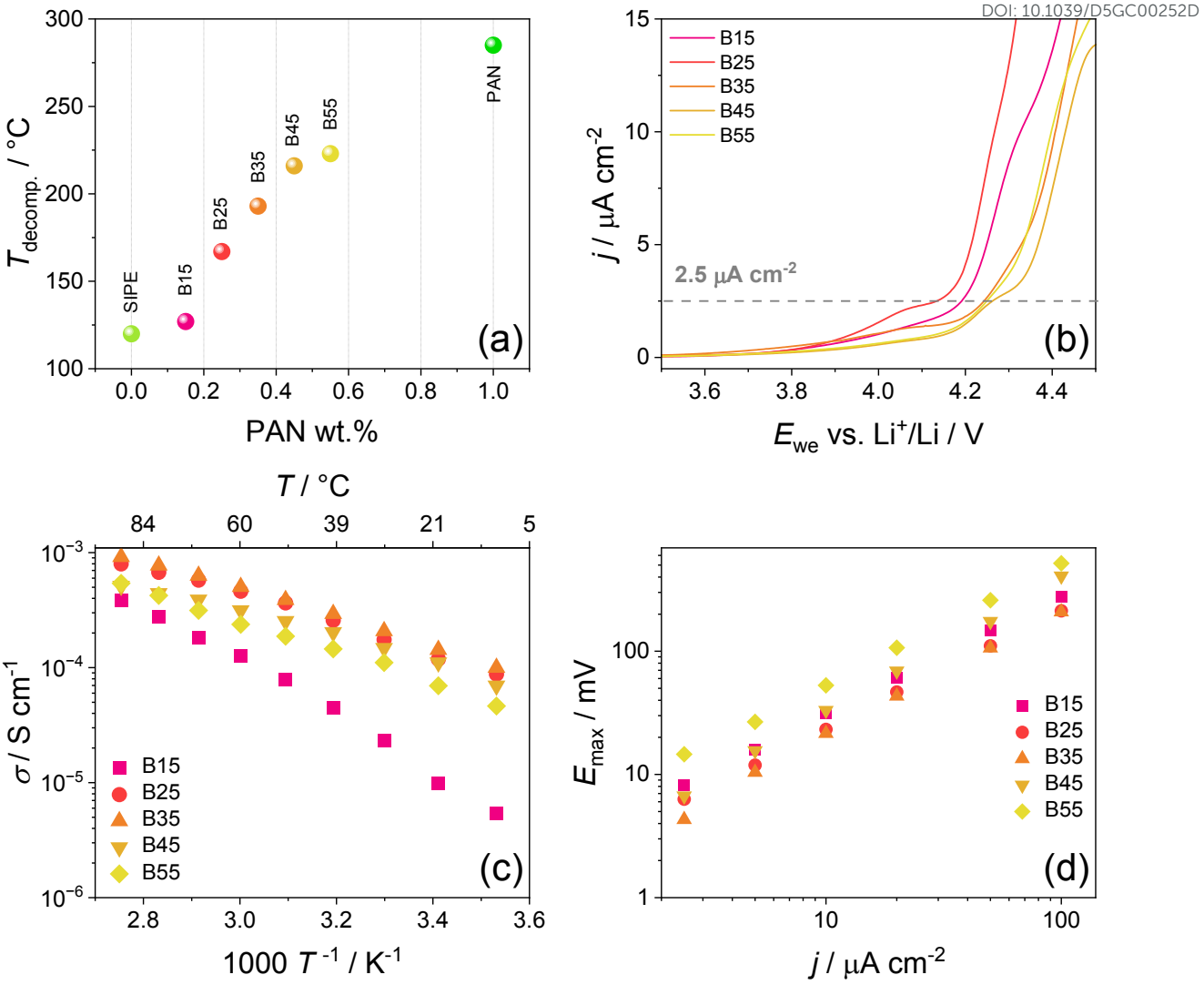

Figure 2. Thermal and basic electrochemical characterization of the B15-B55 membranes: **(a)** decomposition temperature determined via TGA (see **Figure S3**a for the thermograms) and comparison with those of the neat SIPE and bare PAN; **(b)** anodic stability evaluated through LSV between OCV and 6.0 V vs. Li^+/Li using a sweep rate of 0.1 mV s^{-1} at 40 °C; **(c)** Arrhenius plots of the ionic conductivity obtained via EIS (see the Nyquist plots in **Figure S4**) between 10 and 90 °C using the 1.0 MHz – 1 Hz frequency range (voltage amplitude: 10 mV); **(d)** overpotential values related to the Li stripping/plating tests carried out at various current densities at 40 °C (see the corresponding voltage profiles in **Figure S5**).

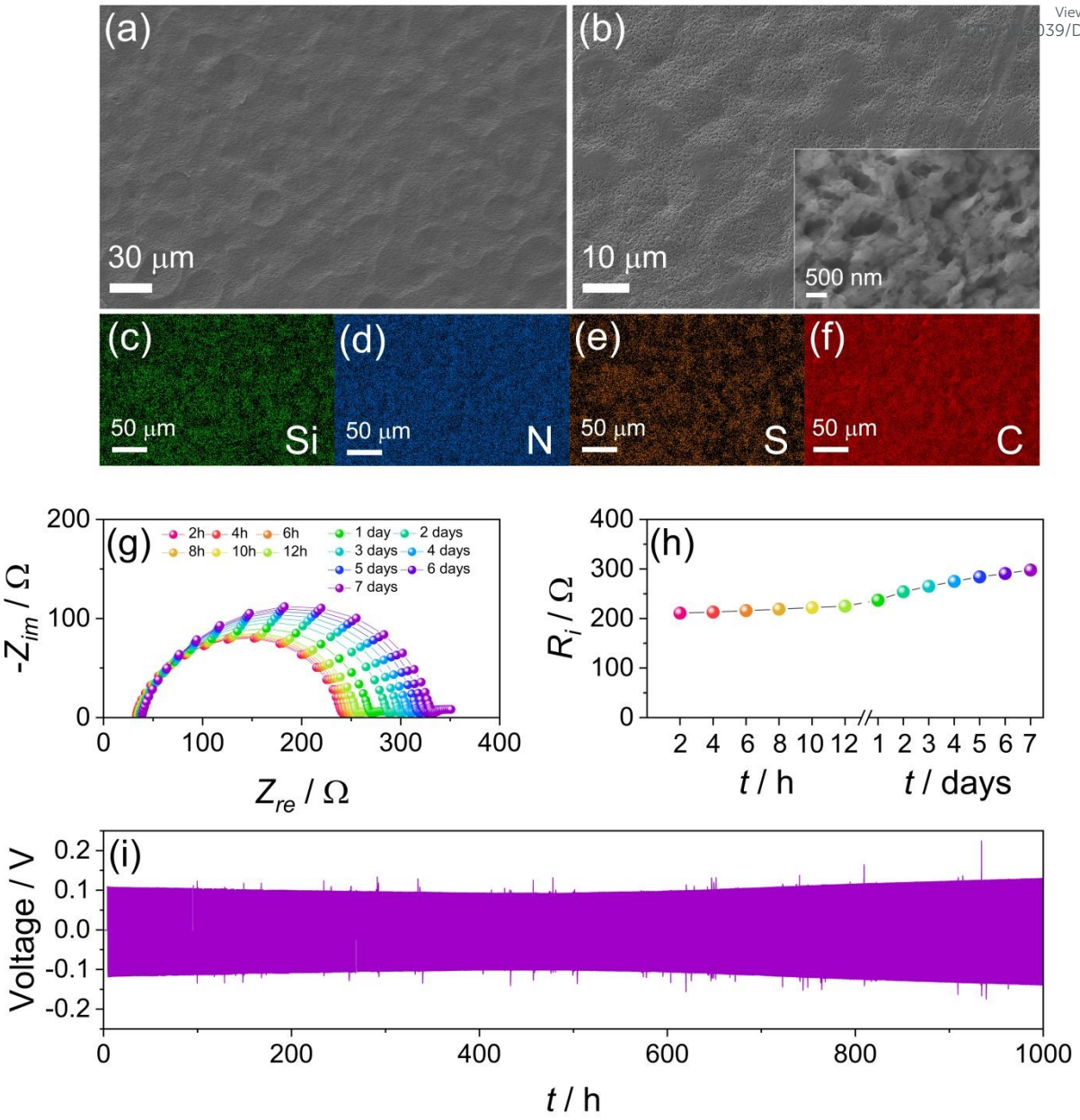

Figure 3. Evaluation of the morphology of B35 and its behavior in symmetric Li‖Li cells: **(a, b)** SEM micrographs at different magnifications and **(c-f) the** corresponding EDX mapping for **(c)** Si, **(d)** N, **(e)** S, and **(f)** C; **(g)** Nyquist plots recorded for a Li‖Li cell in the 200 kHz – 50 mHz frequency range (voltage amplitude: 10 mV) upon calendar aging and **(h)** the trend of the corresponding electrode|electrolyte interphase resistance (R_i) determined through NLLS fitting (see **Table S4** for the actual values); **(i)** voltage profiles related to the long-term Li stripping/plating test performed on a symmetric Li‖Li cells at a constant current density of 50 μA cm^{-2} with a step time of 30 min between charge and discharge. All tests were carried out at 40 °C.

View Article Online
DOI: 10.1039/D5GC00252D

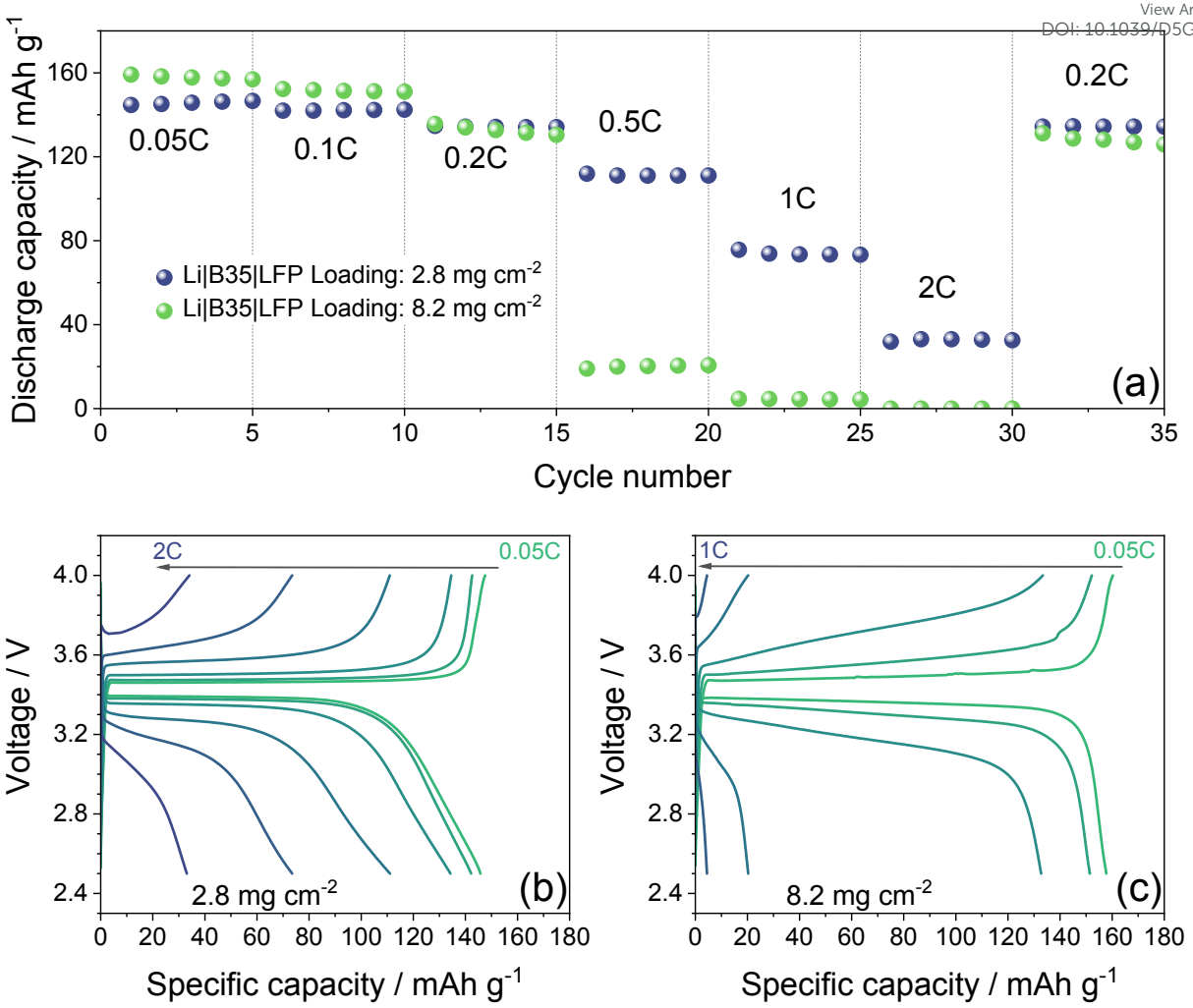

Figure 4. **(a)** Specific capacity as a function of cycle number and **(b, c)** voltage profiles for the rate capability tests performed via galvanostatic cycling on Li | B35 | LFP cells at increasing C rates in the 2.5 – 4.0 V voltage range using an LFP areal loading of either **(b)** 2.8 or **(c)** 8.2 mg cm^{-2}. All tests were carried out at 40 °C.

View Article Online
DOI: 10.1039/D5GC00252D

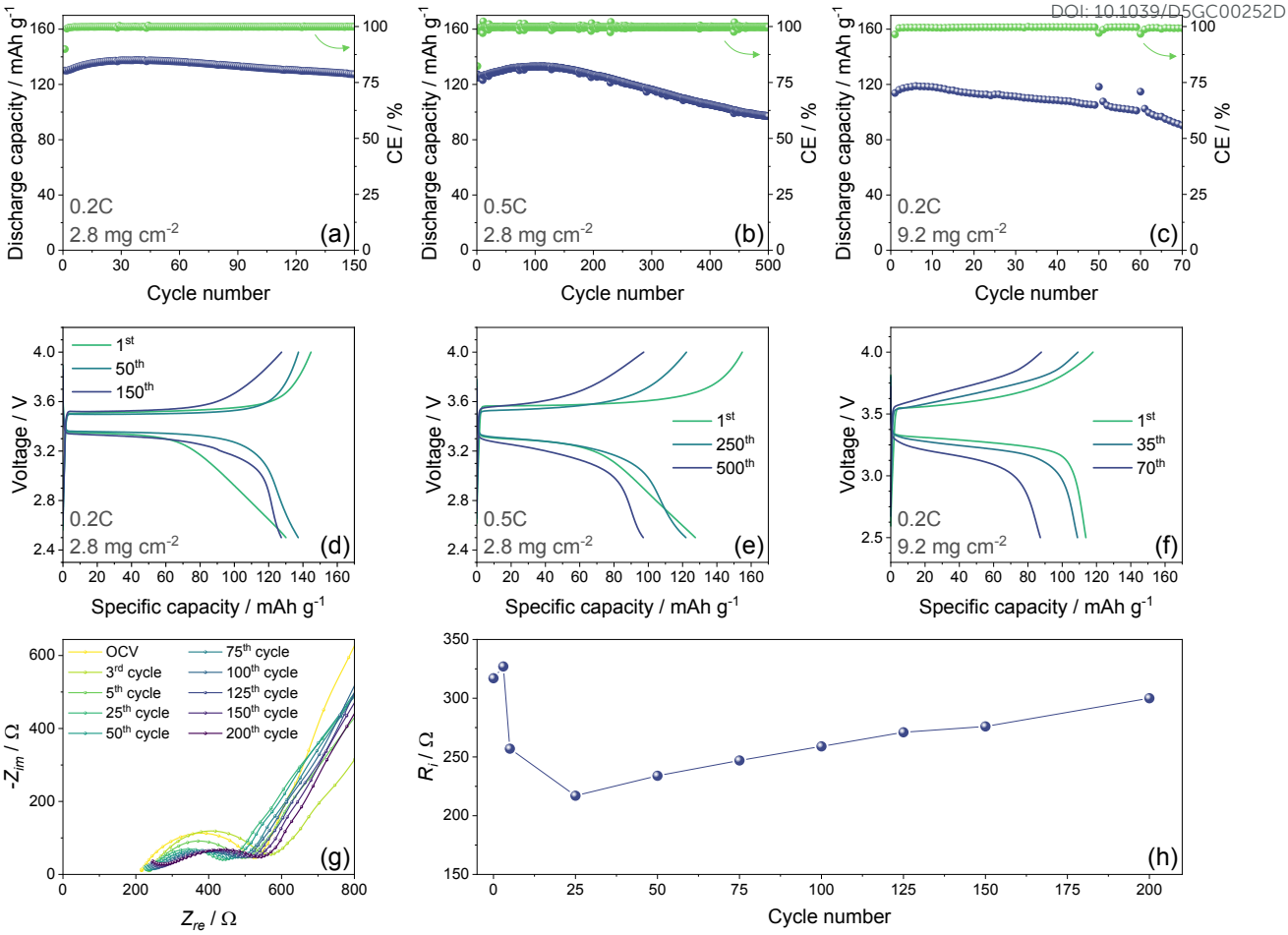

Figure 5. (a-c) Plot of the specific capacity as a function of cycle number (the Coulombic efficiency is displayed on the right *y* axes) and **(d-f)** voltage profiles for the long-term galvanostatic cycling tests performed on Li | B35 | LFP cells with **(a,d)** an LFP mass loading of 2.8 mg cm^{-2} at 0.2C and **(b,e)** at 0.5C, and **(c,f)** with an LFP mass loading of 9.2 mg cm^{-2} at 0.2C. **(g)** Nyquist plots recorded upon cycling of Li | B35 | LFP cells at 0.5C with 3 activation cycles at 0.05C (2.8 mg cm^{-2}) and **(h)** the corresponding trend of R_i as a function of the cycle number obtained by NLLS fitting of the Nyquist plots (the actual data are reported in **Table S6**). Voltage range for cycling tests: 2.5 – 4.0 V; EIS frequency range: 200 kHz – 50 mHz. All tests were carried out at 40 °C.

View Article Online
DOI: 10.1039/D5GC00252D

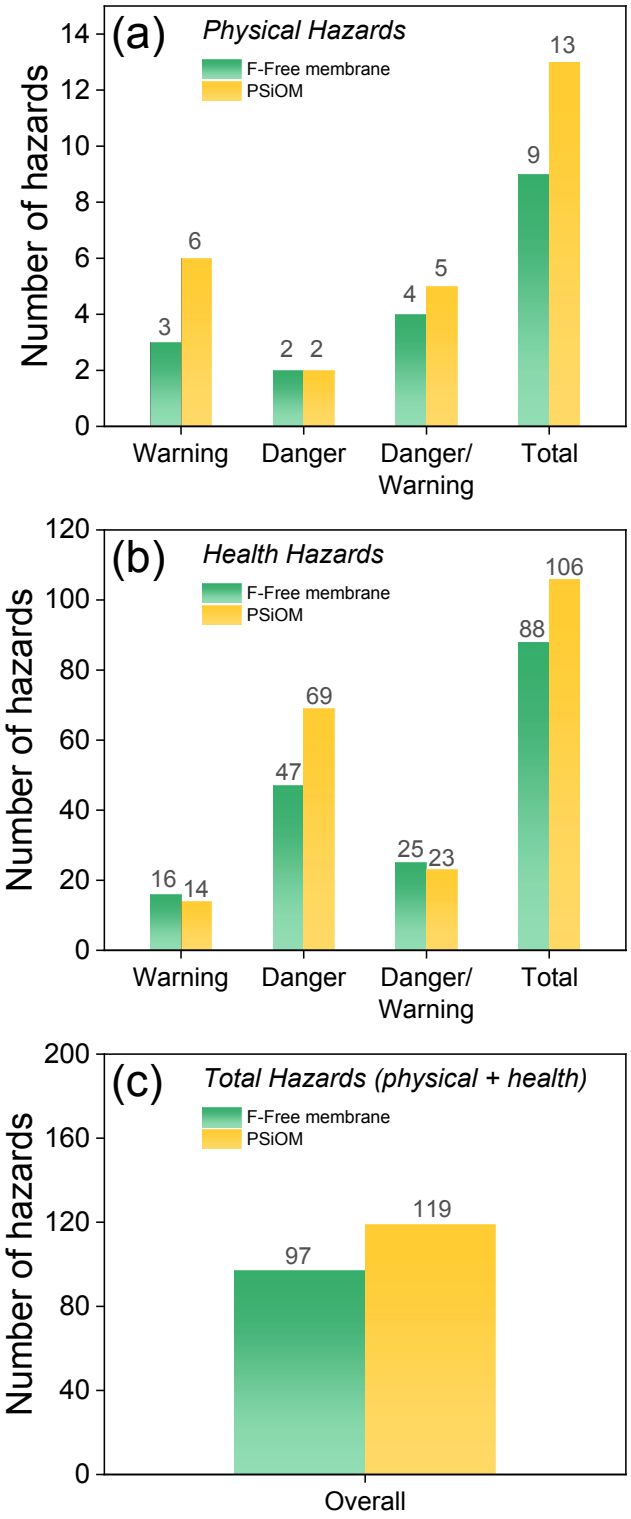

Figure 6. Overview of the number of hazards obtained by the HTL method linked to the F-free SIPE and the F-containing PSiOM (serving as reference) in terms of **(a)** physical, **(b)** health, and **(c)** total hazards (expressed as the sum of physical and health hazards). The detailed HTL results are reported in **Appendix 1** and **Appendix 2** for the F-free SIPE and PSiOM, respectively.

Data availability statements

View Article Online
DOI: 10.1039/D5GC00252D

The data supporting this article have been included as part of the Supplementary Information.